Inferring the effective diffusion coefficient of galactic cosmic rays in the heliosheath

N.B. When citing this work, cite the original published paper.

(article starts on next page)

Inferring the effective diffusion coefficient of galactic cosmic rays in the heliosheath

S. Salvatore [a,b,d,*], S. Della Torre [c], M. Gervasi [c,d], G. La Vacca [c,d], J. Becker Tjus [a,b,e]

[a] *Ruhr-Universität Bochum, Fakultät für Physik und Astronomie, Theoretische Physik IV, Bochum 44780, Germany*
[b] *Ruhr Astroparticle and Plasma Physics Center (RAPP Center), Bochum 44780, Germany*
[c] *INFN Sezione di Milano Bicocca, Milano 20126, Italy*
[d] *Università degli Studi di Milano Bicocca, Milano 20126, Italy*
[e] *Department of Space Earth and Environment, Chalmers University of Technology, Gothenburg 41296, Sweden*

Abstract

The diffusion of Galactic Cosmic Rays (GCRs) into the heliosphere from the local interstellar spectrum is a stochastic process due to the scattering of particles with magnetic irregularities embedded in the solar wind. The process is influenced by energy losses and convection. Our knowledge of the solar wind turbulence properties and dynamics mostly relies on near-Earth and near-Sun observations. The solar wind turbulence behavior is still not well understood when moving far away from the inner heliosphere. Nonetheless, it is still possible to infer some information about the diffusion coefficient by directly probing GCR measurements. In this work, we model the propagation of particles through the heliosheath, i.e. between ~ 90 AU and ~ 120 AU distance from the Sun, solving the Parker transport equation by means of a numerical Monte Carlo technique. We apply a data-driven approach based on *in situ* observations from Voyager 1 in order to study the solar modulation for different particles and derive the diffusion coefficient rigidity dependence. To do this, the most abundant elements in the solar system are considered together with their corresponding isotopes. We conclude that the effective diffusion coefficient, in the energy range from 0.04 to 0.31 GeV/nuc, has a rigidity dependence of P^γ with $\gamma \sim 1.42^{+0.63}_{-0.42}$. This result can be used to constrain the spectral behaviour of the turbulence in the heliosheath.
© 2025 The Author(s). Published by Elsevier B.V. on behalf of COSPAR. This is an open access article under the CC BY license (http://creativecommons.org/licenses/by/4.0/).

Keywords: Turbulence; Diffusion coefficient; Galactic cosmic rays

1. Introduction

It has been more than a century since the first detection of cosmic rays. Still, their origins are largely unknown. One of the largest problems with identifying the sources of cosmic rays is that they react to interstellar, as well as interplanetary and intergalactic magnetic fields, often propagating diffusively (e.g Tjus and Merten, 2020). This way, the cosmic-ray flux as detected at Earth loses all its information about the original direction of the particles, and indirect observables like gamma-ray or neutrino measurements are the only way to deduce information about the high-energy cosmic rays (e.g. Reichherzer et al., 2022). Galactic Cosmic Rays (GCRs) at an energy below ~ 30 GeV/nuc are even influenced significantly by the magnetic heliosphere of the Sun (Stone et al., 2013; Bobik et al., 2016; Rankin et al., 2022). This process is known as solar modulation (Moraal, 2013; Boschini et al., 2018b; Song et al., 2022). Measurements of GCR intensity at several solar distances are provided by the Voyager probes

---

* Corresponding author.
E-mail addresses: silvia.salvatore@rub.de (S. Salvatore), stefano.dellatorre@mib.infn.it (S. Della Torre), massimo.gervasi@unimib.it (M. Gervasi), giuseppe.lavacca@unimib.it (G. La Vacca), julia.tjus@rub.de (J. Becker Tjus).

(Richardson, 2013; Cummings et al., 2016; Hosteaux et al., 2022; Kurth et al., 2023). At the energies detected by Voyager the majority of the solar modulation occurs in the heliosheath (Boschini et al., 2019). This peripheral region of the heliosphere is internally bounded by the termination shock - i.e. the region where the solar wind suddenly slows down passing from a supersonic to a subsonic regime - and externally by the heliopause - i.e. the true heliosphere boundary, corresponding to the limit of the solar wind expansion. Outside of the heliopause, the local interstellar medium dominates (Fraternale et al., 2022). The heliosheath is a very turbulent region. Here the main source of energy is provided by the pick-up ions (PUIs) (Fraternale et al., 2022; Sokółet al., 2022). The PUIs are created by the ionization processes of interstellar neutral atoms occurring in the solar wind mainly in the inner part of the heliosphere, i.e. the region inside the termination shock. The ionized interstellar neutral atom is then "picked up" by the magnetic and motional electric field of the solar wind plasma which incorporates the PUI at highly non-thermal speeds in the reference frame of the solar wind (Zirnstein et al., 2022). The plasma speed, density, and temperature fluctuate throughout the heliosheath. The magnetic field fluctuations, influenced by solar activity, are generating turbulence in the medium, which is much larger in the heliosheath with respect to the inner heliosphere. Voyager 2 magnetic field measurements in the heliosheath show that magnetic field changes can occur on a temporal scale of 10–20 min, corresponding to length scales of 60,000–120,000 km (determined from the speeds measured by the Voyager 2 plasma instrument). To provide an idea of the turbulence scale in terms of the energetic PUIs, it is worth reminding that the Larmor radius of a 1 keV (4 keV) pickup proton is ∼30,000 km (∼60,000 km), corresponding to a period of 5 min (10 min) (Richardson and Burlaga, 2013). Thus, some information on the turbulence spectrum in the medium mostly comes from the observations of the two Voyager spacecraft.

Reviews of how the solar modulation is occurring in the heliosphere, through observations of GCR intensities, and on the models describing such phenomena can e.g. be found in Rankin et al. (2022) and Engelbrecht et al. (2022), respectively. For the purpose of this work, we recall that the Parker Transport Equation (PTE) is the standard approach for particle propagation in the heliosphere (Parker, 1965). This equation describes the particle transport as due to convection, diffusion, and energy-changing processes combined in the form of a Fokker-Plank-like transport equation. The key point of the model is represented by the description of the diffusion process as a magnetic scattering of charged particles on the turbulent fluctuations of the Interplanetary Magnetic Field (IMF). The IMF is mainly generated by the Sun's magnetic field that is carried out with the outward-flowing solar wind plasma (Rao, 1972).

Over the last few decades, several analytical and numerical models have been developed to describe the turbulence cascade from the injection to the dissipation scales, which led

to different predictions on the scaling of the magnetic energy spectra (see, e.g., Fahr et al., 1986; Zank, 1999; Borovikov, 2008; Borovikov, 2012; Huang et al., 2021). The study of the magnetic turbulence in the interplanetary medium, in principle, could allow one to derive the mean free path (MFP) of cosmic ions and, in turn, the coefficients of the diffusion matrix in the PTE (see Jokipii (1971) for the original idea and Reichherzer et al. (2020), Reichherzer et al. (2022) for new work). Many models use a magnetohydrodynamic (MHD) approach where simulations for the parallel $k_{\parallel}$ and perpendicular $k_{\perp}$ components of the diffusion tensor K are performed, in different conditions (Florinski et al., 2003; Luo et al., 2015; Lemoine, 2023; Reichherzer et al., 2025). Almost all the theoretical models focus on the inner heliosphere (e.g. Jokipii (1971), Rao (1972), Caballero-Lopez et al. (2019)). In this work we use an empirical approach, combining PTE solutions along with high precision GCRs measurements in space (see, e.g., Boschini et al., 2018b; Boschini et al., 2019), to study the rigidity dependence of the diffusion coefficient in the outer part of the heliosphere, the heliosheath. At present, there are several attempts to develop an *ab initio* theory for deriving the PTE diffusion matrix, but these will require further advances in turbulence transport modelling, and further improvements in our understanding of cosmic ray transport coefficients, given the differences in values for these quantities yielded by various theories discussed in Section 5.2. of Engelbrecht et al. (2022, and reference therein). This work aims to help constrain the rigidity dependences in the theoretical models, by providing a simplified yet reasonable formula for the diffusion coefficient in the heliosheath without accounting for the complex description of the turbulence theoretical details in such area. In order to do this, we use HelMod (Boschini et al., 2017; Boschini et al., 2018a; Boschini et al., 2019; Boschini et al., 2020), which treats the diffusion in the heliosphere in a different way, whether the particle is within the termination shock or beyond it. When the cosmic rays are in the inner heliosphere, the approach is two-dimensional, and $k_{\parallel}$ and $k_{\perp}$ are set to the values provided in Boschini et al. (2019) (see Appendix A). For the heliosheath, a simplified one dimensional description is used. The two + one dimensional approach has been proven to work well, as HelMod is able to reproduce the GCRs modulated spectra at 1 AU successful. In our study we modify the diffusion coefficient in the heliosheath provided in Boschini et al. (2019) in order to modulate the GCR local interstellar spectra (LIS) and make them fit the Voyager 1 observations at different rigidity bins. Section 2 describes the transport model with a focused discussion on the heliosheath. Section 3 and Section 4 present the analysis methodology and the discussion of the so obtained results.

2. Particle diffusion in the Heliosheath

As pointed out by Parker 1965, charged particle propagation through interplanetary space is dominated by the magnetic collisions with the small scale irregularities of

the IMF. The resulting phenomenon is a Markov process that can be described as a diffusion mechanism by means of the PTE (Parker 1965). On the collision length scale - i.e. the average magnetic collision distance - one can see the diffusion process as a stochastic motion whose effective propagation can be described by means of the MFP; in turn, this quantity could be easily related to the diffusion coefficient in the PTE (Jokipii, 1971).

In recent years, significant theoretical advances have been made in our understanding of how solar wind turbulence influences the diffusion of charged particles (see Engelbrecht et al., 2022, for a theoretical review). We know that the power spectrum of magnetic irregularities can be related to the diffusion tensor through a statistical approach presented in detail by Jokipii (1971). Thus, an energy (or rigidity P) dependence of the diffusion coefficient can be inferred. There are many models proposed in literature for both the parallel and perpendicular components of the diffusion coefficient in the diffusion tensor. Following Jokipii (1971), we have $k_{\parallel} \propto \beta P^{1/2}$ for $P < P_{\text{th}}$ and $k_{\parallel} \propto \beta P^2$ for $P > P_{\text{th}}$, with a threshold rigidity $P_{\text{th}} = 1$ GV and the term $\beta = v/c$ defining the particle velocity normalised to the speed of light. The perpendicular component is then, only for $P < P_{\text{th}}$, expected to follow this behaviour: $k_{\perp} \propto \beta$. Rao (1972) instead proposed $k_{\parallel} \propto \beta$ for $P < P_l$ and $k_{\parallel} \propto \beta P^{2-q}$ for $P_l < P < P_u$. Hereby, P_l is the particle rigidity for which the mean free path becomes smaller and approaches the correlation length of the interplanetary magnetic field, P_u is the rigidity at which the gyro-radius r_{g} of the particle becomes approximately equal to the scattering mean free path given by $\lambda = 3k_{\parallel}/c\beta$ and q is the spectral index of the turbulence transverse component. The change in slope is expected at ~ 2 GV. Then, the perpendicular component is given by $k_{\perp} = k_{\perp}^{\text{m}} + (r_{\text{g}}^2/\lambda^2)k_{\parallel}$. The first term represents the contribution due to the random walk of field lines and the second one the resonant scattering by field fluctuations. Caballero-Lopez et al. (2019) provided yet another option for the modeling of the diffusion coefficient: $k_{\parallel} \propto \beta P^{1/3}$ for $P < P_{\text{th}}$ and $k_{\parallel} \propto \beta P^2$ for $P > P_{\text{th}}$, while $k_{\perp} \propto \beta P^{1/9}$ for $P < P_{\text{th}}$ and $k_{\perp} \propto \beta P^{2/3}$ for $P > P_{\text{th}}$, with $P_{\text{th}} = 1$ GV. All of these models, presenting a flatter behavior at low rigidities and harder spectra for rigidities $P > P_{\text{th}} \sim 1 - 2$ GV, are focused on the inner heliosphere. Hereby, we assume the diffusion coefficient in the heliosheath to show a similar behaviour, i.e.

$$\kappa \propto \begin{cases} \beta P^{\alpha} & \text{if } P < P_{\text{th}} \\ \beta P^{\epsilon} & \text{if } P > P_{\text{th}} \end{cases}$$

where α and ϵ are expected to differ from one another. A quasi linear ($\epsilon = 1/3$) dependence at higher rigidities is expected for the regime of small turbulence, i.e. $\delta B/B < 1$. In this case, the turbulence behaviour comes from the Kolmogorov spectrum. For $\delta B/B \gg 1$, instead, we observe the Bohm regime ($\epsilon = 1$). A transition from the quasi linear regime to the Bohm regime is expected in

between (e.g. Reichherzer et al., 2020). A more general form for the diffusion coefficient also includes solar distance dependence and could be written in the form of (see, e.g. Engelbrecht and Di Felice, 2020, and reference therein)

$$\kappa(r, P) = \frac{\beta c}{3} \lambda_0 \left(\frac{r}{r_0}\right)^{\alpha} \left(\frac{P}{P_0}\right)^{\delta} \tag{1}$$

with λ_0 some effective mean free path value at distance r_0 and rigidity P_0. This parametrisation is relatively simple and mimics the form often used in modulation studies. It is important to note that, in this formulation, the spatial dependence of κ in the inner heliosphere is most probably due to the radial evolution of turbulence (see, e.g. Pine et al., 2020a; Pine et al., 2020b; Pine et al., 2020c; Pine et al., 2020d; Pine et al., 2020e, for measurement in the inner heliosphere), while the rigidity dependence is most probably related to the power spectral density of the IMF (see, e.g. Jokipii, 1971).

Much of our current knowledge on turbulence in the inner heliosheath has been acquired via *in situ* observations made by Voyager spacecrafts but the turbulence behaviour in this region is still poorly understood, from both the observational and the theoretical perspectives (some theoretical studies can be found in e.g., Goldstein et al., 2015; Kleimann et al., 2022). Observations are limited to 1D measurements by Voyager but there is a lack of plasma data and interstellar PUI (Fraternale et al., 2022) observations, together with a high level of noise in the measurements. The PUIs -with a temperature of $\sim 10^6$ K (Sokół et al., 2022) - dominate the thermal pressure of the solar wind beyond 30 AU and cause the plasma temperature in the heliosheath to range from 50,000 to 150,000 K. The turbulence here is much more complex than in the supersonic solar wind because of the lower bulk wind speed - i.e. $v_{\text{sw}} \sim 150$ km/s in the heliosheath (Fraternale et al., 2022) compared to $v_{\text{sw}} \sim 750$ km/s in the polar regions of the inner heliosphere during low solar activity periods (McComas et al., 2008). In addition, there are shocks and, possibly, fluctuations of dispersive nature whose propagation speed is affected by the energetically dominant population of PUIs (Fraternale et al., 2022).

2.1. Numerical model

In the heliosheath, although Voyager 2's solar wind speed measurements do not show a significant dependence on radial direction (Richardson, 2013), the radial component of the flow progressively slows down at a rate of $1/r^2$ as it moves toward the stagnation point (see Fig. 2 in Boschini et al., 2019; Scherer et al., 2011). Therefore, the solar wind plasma flow can be approximated as incompressible and divergence-free. This means that adiabatic energy losses are negligible in this region.

When it comes to particle drift, understanding the geometry of the heliospheric magnetic field and the wavy

structure of the heliospheric current sheet in the heliosheath is significantly more difficult than in the inner heliosphere (Burlaga et al., 2007; Borovikov et al., 2011). As a result, there is no consensus on the importance of particle drifts within the heliosheath (Potgieter, 2013; Manuel et al., 2014). It is generally believed that increased turbulence and a less organized heliospheric magnetic field occur downstream of the termination shock, which leads to a reduction in drift effects (Fraternale et al., 2022). Therefore, in the "effective" radial one-dimensional treatment of solar modulation in the heliosheath presented in this work, the drift effect has been neglected as a first approximation.

We describe the particle propagation in the heliosheath by means of a spherical symmetric PTE as decribed in Section 5 of Boschini et al. (2019).

$$\frac{\partial U}{\partial t} = \frac{1}{r^2}\frac{\partial}{\partial r}\left(r^2\kappa\frac{\partial}{\partial r}U\right) - \frac{1}{r^2}\frac{\partial r^2 v_{\text{sw}}U}{\partial r} \tag{2}$$

where U is the number density of particles with respect to kinetic energy per nucleon, t is the time coordinate, r is the radial distance, κ is the diffusion coefficient and v_{sw} is the radial solar wind bulk speed in the heliosheath.

Langner and Potgieter (2005) proved that the approximation of a symmetrical heliosphere, although it is simplified, is justified when studying the external layer, i.e. the heliosheath (Kleimann et al., 2022). Moreover, the region of interest is probed by Voyager 1 in the nose direction, which is only a bit compressed, if compared to the tail direction. For that one, a greater asymmetry is still debated. The model we use is fully described in Boschini et al. (2019).

As described in Boschini et al. (2019), in order to account for the strong modulation effect observed by Voyager 1 in 2012 before the heliopause crossing (see, e.g. Zhang et al., 2015, and rereference therein), the diffusion coefficient must be reduced by a factor 50 in the outermost layer, 1–2 AU thick, thus allowing the creation of a diffusion barrier against low energy CRs propagation.

The PTE can be transformed to a Fokker Planck equation, which generally can be expressed in terms of a set of stochastic differential equations (SDEs). The SDEs can be cast into the general form

$$\frac{dx(t)}{dt} = a(x,t) + b(x,t)\zeta(t) \tag{3}$$

where x stands for the position coordinate, $a(x,t)$ and $b(x,t)$ are continuous functions and $\zeta(t)$ represents a rapidly varying stochastic function in time. $a(x,t)$ is usually referred to as the deterministic term, while $b(x,t)$ is the diffusion term. Here, SDEs of the Itō type are considered, where Eq. (3) can be rewritten as

$$dx(t) = a(x,t)dt + b(x,t)dW(t) \tag{4}$$

with $W(t)$ representing the Wiener process, i.e. a time stationary stochastic process where the time increments have a normal distribution with a zero mean and a variance

equal to dt, $dW(t) \sim N(0,dt)$ (Strauss and Effenberger, 2017). In a backward in time approach, instead of following the position of the particles - i.e. $x(t)$ - from the interstellar medium to Earth, we reverse the time coordinate. Thus, the numerical process starts from the target in a generic position in the heliosphere with a fixed initial kinetic energy or momentum and traces back quasi-particle objects till the heliosphere boundary, gaining energy in the region inside the termination shock. We use the Voyager 1 probe for the solar modulation data. The spacecraft has travelled from the heliosphere to the interstellar medium, collecting ions data throughout its journey. Therefore, in this framework, the target for the backward in time approach is represented by the Voyager 1 probe observations at the different positions reached throughout its trajectory in the heliosphere. We follow the evolution of the particles towards the outer heliosphere.

In the zone of interest, in order to reproduce the form of Eq. (4), the SDE is (Bobik et al., 2016)

$$dr = \left(\frac{2\kappa}{r} - v_{\text{sw}}\right)dt + \sqrt{2\kappa}dW \tag{5}$$

where dt stands for a backward in time step and dW expresses a standard Wiener process with variance equal to 1. This diffusion term represents the diffusion of particles in the magnetic field of the heliosheath. For the deterministic term, we need to account for the convection speed with a minus sign $-v_{\text{sw}}$ since the solar wind is directed outwards. When the process is dominantly stochastic, i.e. of diffusive nature[1], we can evaluate through a Monte Carlo procedure the normalized probability function $G(P_0|P)$ that gives the probability for a particle observed at Earth with a rigidity P_0 having a rigidity P at the heliospheric boundary. Once $G(P_0|P)$ is evaluated it is possible to obtain the modulated spectrum directly from $J_{\text{LIS}}(P)$, the Local Interstellar Spectrum of the considered isotope. Local interstellar spectra are provided by Boschini et al. (2020), using GALPROP (Strong and Moskalenko (1998), webpage: https://galprop.stanford.edu/). The isotopic contribution is included in the LIS for each nuclear species (Boschini et al., 2017) and accounted for when converting from kinetic energy to rigidity. We point out that an under/overestimation on the LIS can bias the resulting modulated calculated spectra.

3. Methodology

3.1. Data preparation and procedure

In the present study, we consider the six most abundant cosmic ions observed by Voyager 1 from the beginning of 2000 up to the end of 2016: H, He, C, O, Mg and Si. This interval is chosen in order to cover the whole period spent

---

[1] In order to solve Eq. (5) in the so called *diffusion approximation*, we check that ds is such that the diffusion process is dominant with respect to the advection process, i.e. $\sqrt{2\kappa}dW \gg \left(\frac{2\kappa}{r} - v_{\text{sw}}\right)ds$.

by the Voyager probe inside the heliosheath, considering also the period immediately before crossing the termination shock and after crossing the heliopause. This is done in order to have some constraint with the experimental data at the boundaries of the heliosheath. The data are averaged over 3 Carrington rotations[2], in order to reduce the statistical experimental errors. We simulate 24 rigidity bins, considering each isotope separately, and the final spectra are computed by summing the modulated isotope spectra.

By comparing the simulation outcomes with the Voyager 1 experimental data over the whole time span and accounting separately for each rigidity bin, we obtain the best-fit values of κ (for each cosmic ion population). Following the prescription by Boschini et al. (2019), we test a grid of κ values between 0.5×10^{-5} and 4×10^{-5} AU^2 s^{-1}. For each simulation run, the goodness of the simulated time-dependent spectra with respect to the corresponding time-dependent Voyager 1 observation is evaluated by means of the χ^2 test. The number of injected particles has been chosen in such a way that the error on the model is much lower than the statistical uncertainties of experimental data. Thus, computational artifacts from the model become negligible. In Fig. 1 we report the simulations set with the best agreement with the Voyager 1 data for a rigidity of 0.59 GV in the case of Si and 0.82 GV for H.

The results of the κ scan are reported in Fig. 2, as a function of κ with rigidity. Similar values of κ are found at the same rigidities, but for different ions (reported with different colors). We notice three values, all corresponding to protons, that are not following the global trend for the diffusion coefficient behaviour. Nonetheless, we assume these to be simply fluctuations over the whole studied range. These findings, considering the uncertainties of current data, indicate a universality in the rigidity dependence of the different nuclei in the cosmic-ray spectrum in the rigidity range of $\sim 0.5 - 2$ GV, as expected from basic theory.

3.2. Interpretation

The points in Fig. 2 are interpolated with a power law equation in the generic form:

$$\frac{\kappa}{10^{-5}\beta} = a\left(\frac{P}{1\text{GV}}\right)^{\gamma} + c \tag{6}$$

where γ is the spectral index of the rigidity dependence, and a and c are the fit parameters, in units of AU^2 s^{-1}. This form is derived by Eq. (1) where we focus on the rigidity dependence. Due to the large distance of the heliosheath

from the Sun and the relatively small radial dimensions with respect to the inner heliosphere, together with the fact that in the heliosheat the turbulence is much compressed, we estimate that a radial dependence would introduce at worst a 30 % uncertainties in our estimation, that is below the intrinsic uncertainties due to the scatter of points in Fig. 2. Moreover, Voyager's data covers more than 7 years of data taking so that the κ value obtained from this procedure (which aims to fit the whole dataset with the same value of the parameters) should be considered as an effective diffusion coefficient that, in principle, may change with time masking smaller effects due to radial dependence. In additon, we avoid to test the broken power law around P_{th}, due to the limited rigidity span covered by Voyager observations.

The interpolation procedure uses a Markov Chain Monte Carlo bayesian approach following the one presented in Goodman and Weare (2010) and implemented with the emcee python package. This is done in order to provide some confidence band around the parameters of the model, given that there are no error bars on the values plotted in Fig. 2.

The assumed priors on a, c and γ are given by uniform probability distributions in the following ranges (roughly covering the values in the literature for similar rigidity dependence): $a/10^{-5} \in [0.1, 2.9]$ AU^2 s^{-1}, $c/10^{-5} \in [0.2, 2]$ AU^2 s^{-1} and $\gamma \in [0.2, 3]$.

We assume, for the calculation of the posteriors on the parameters a, γ and c, that the errors on the diffusion coefficient values κ present a normal distribution with $\sigma = 1$. This value is coming from the biggest fluctuation in κ found between two adjacent rigidity bins ($\Delta\kappa \approx 0.85$ between the ~ 0.651 GV bin for the proton and the ~ 0.656 GV bin for the O ion). Although this is clearly an overestimation of the uncertainties for all the bins, we fix the priors for σ_{n} to that value and treat them as nuisance parameters. This assumption allows us to compute the likelihood function in terms of the model θ and the data D such as

$$\log(P(D|\theta)) = -\frac{1}{2}\sum_{n}\left[\frac{(\kappa_n - \kappa_{\text{model}})^2}{\sigma_n^2} + \log(2\pi\sigma_n^2)\right] \tag{7}$$

Hereby, κ_{model} is the model fit to the κ_n values and the σ_n are the errors. The previous assumption is a strong hypothesis on the κ error distribution. The outputs of the fitting procedure are the one and two dimensional projections of the posterior probability distributions of the a, c and γ parameters (see Fig. 3 on the left). Comparison between the best fit power law and best fit κ values are shown in Fig. 3 right panel. Technical details of the procedure can be found in Salvatore (2023). The intervals defining the CLs for the one dimensional posteriors are drawn considering the 16th and the 84th percentiles of the distributions; these levels determine the 68 % CL region. The so called corner plot, instead, shows the two dimensional projections of the posterior probability distributions correlating the

---

[2] The differential rotation depends on the solar latitude with a duration of ~ 25 days on the Sun's equatorial regions and of ~ 35 days on the polar regions. Richard C. Carrington defined a fixed solar coordinate system that rotates in a sidereal frame exactly once every 25.38 days. Since the observer is on Earth, which itself revolves around the Sun, the synodic period of a Carrington rotation varies slightly during the year, with an average of 27.2753 days. Periods of ~ 27 days will be referred to as a single Carrington rotation throughout this work (Low, 2019).
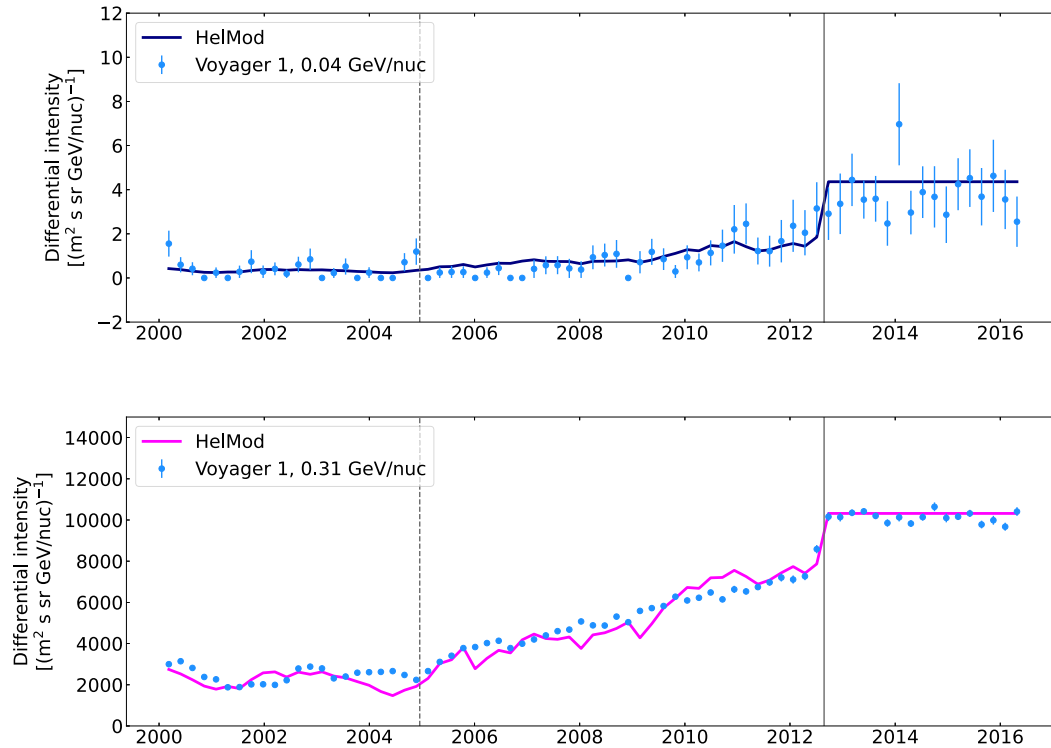
Fig. 1. Time modulated spectra for rigidity 0.59 GV (Si, upper panel) and 0.82 GV (H, lower panel) along with Voyager 1 data (the data were extracted in March 2021 from https://voyager.gsfc.nasa.gov/flux.html). The termination shock and heliopause positions are also indicated in the plot as a vertical line (dashed and solid respectively).
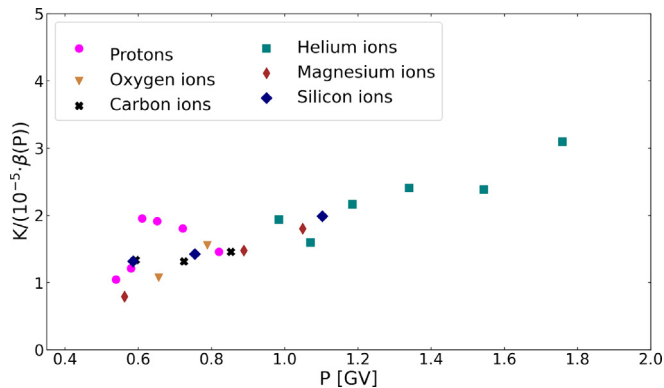

Fig. 2. Computed values of diffusion coefficient κ in the heliosheath. Each point represents the value corresponding to the best agreement of the time distribution with the Voyager 1 data (the data were extracted in March 2021 from https://voyager.gsfc.nasa.gov/flux.html).

parameters a, c and γ. Looking at the posteriors, we notice that the distributions are not gaussian-like, but are asymmetrical. This could possibly be due to the assumption on the errors on the κ_n values. Nonetheless, assuming a gaussian shape for the uncertainty around the κ values allows us to provide some reasonable results in terms of the rigidity dependence of the diffusion coefficient. Thus, we stick to this procedure and use it for a linear model as well, i.e. $\frac{\kappa}{\beta} = aP + c$, since the result for the γ value with the power law is consistent with unity (see Fig. 4 for the results). From now on, we will use the 68 % CL region around the parameters as an estimate of their error.

To discriminate between the two models, due to the small ($N = 24$) size of the sample, a Student's t-test is computed in both cases to provide a *p*-value for the fits (Lista et al., 2017).

In the case of a linear function we derive a *p*-value of 91 % while with the power law function the *p*-value is equal to 99 %. This suggests that, although both models would produce a good agreement, there is a small preference for the power law function with $\gamma = 1.42$ (see Table 1 for the best fit parameter values).

As a final investigation, we apply both these functional forms to the diffusion coefficient κ and compute the simulated spectrum for the AMS-02 data using the LIS described in Boschini et al. (2020) and, for the inner heliosphere propagation, the description in Boschini et al. (2019).

A representative example is reported in Fig. 5. The modulated spectrum is consistent with what was obtained by Boschini et al. (2019, 2020); on the other hand, this result shows that for high rigidity a different spectral index of the diffusion coefficient in the heliosheath has a minimal impact on observations at 1 AU.

4. Discussion and conclusions

Throughout this work, the rigidity dependence for the diffusion coefficient in the heliosheath is inferred using a Monte Carlo numerical solution of the particle transport equation and a practical data driven approach.
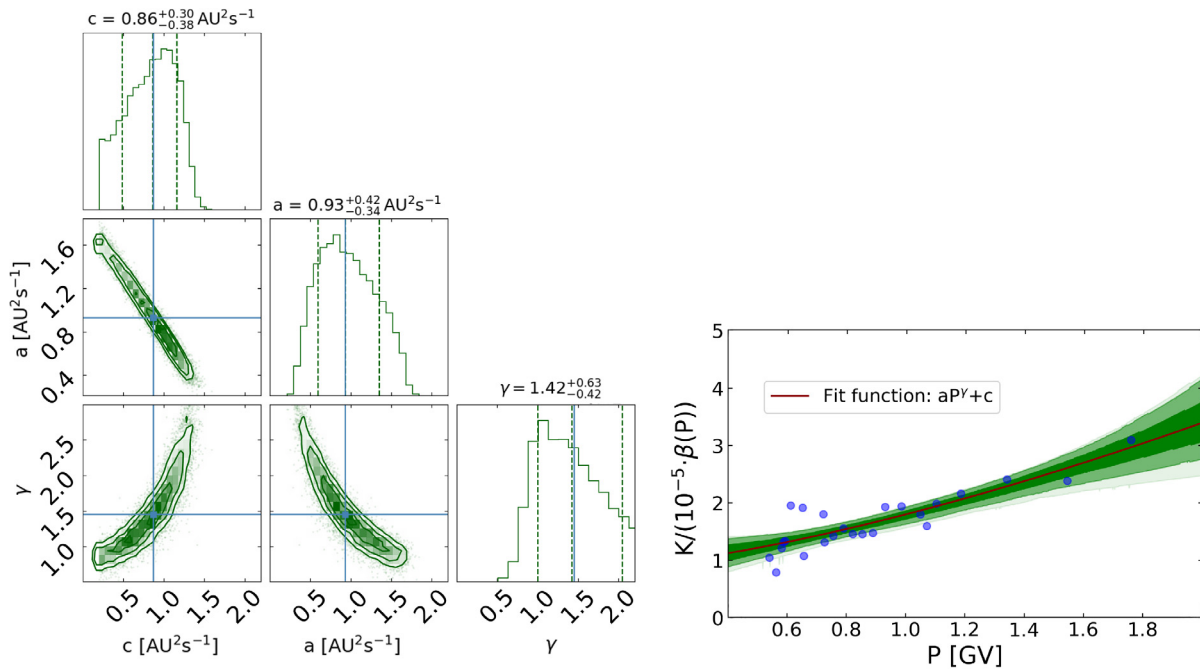
Fig. 3. Left: One and two dimensional projections of the posterior probability distributions of the a, c and γ parameters derived through the bayesian approach for a generic power-law function. The vertical dashed lines indicate the 16th, 50th and 84th percentiles of the samples, which correspond to the 68 % CL region around the derived value for each parameter. The blue lines indicate the values of the parameters derived from the least squares method fit procedure. Right: Best fit function (defined as the median values of parameters) applied on data along with the 68 %, 95 % and 99 % confidence level regions (drawn with different shades of green). (For interpretation of the references to colour in this figure legend, the reader is referred to the web version of this article.)
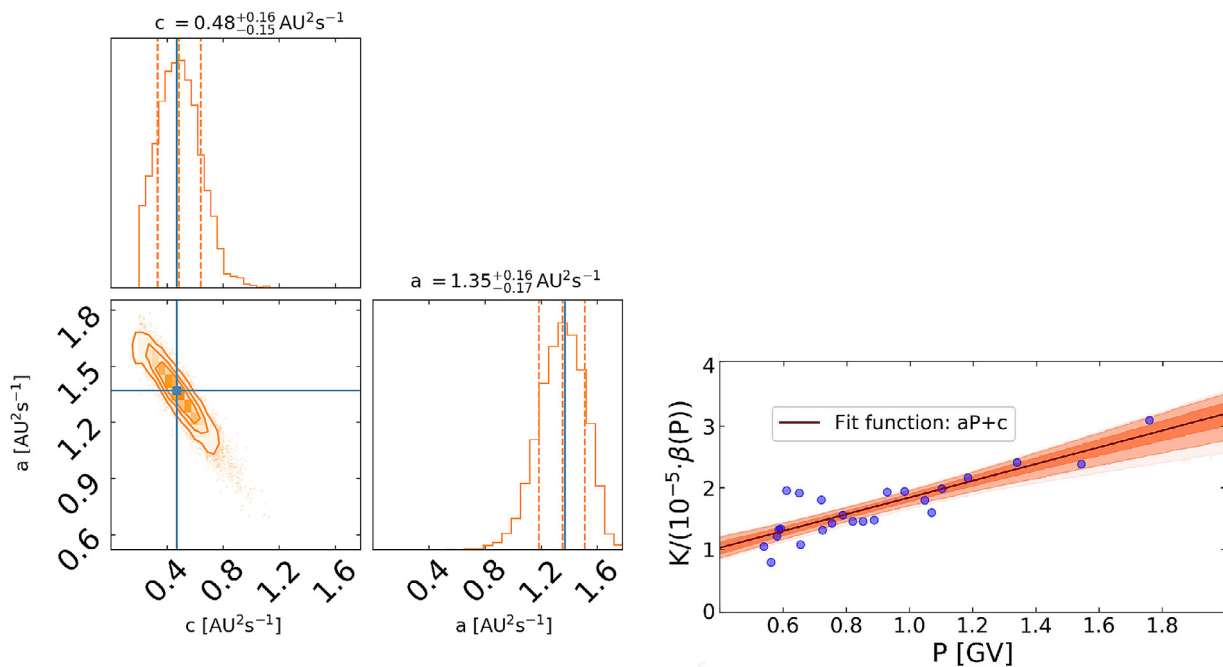

Fig. 4. Left: One and two dimensional projections of the posterior probability distributions of the a and c parameters derived through the bayesian approach for a generic power-law function. The vertical dashed lines indicate the 16th, 50th and 84th percentiles of the samples, which correspond to the 68 % CL region around the derived value for each parameter. Right: Best fit function (defined as the median values of parameters) applied on data along with the 68 %, 95 % and 99 % confidence level regions (drawn with different shades of orange). (For interpretation of the references to colour in this figure legend, the reader is referred to the web version of this article.)

Table 1
Best fit parameters.

Power law	Linear model
$a = 0.93^{+0.42}_{-0.34}$ AU^2 s^{-1}	$a = 1.35^{+0.16}_{-0.17}$ AU^2 s^{-1}
$c = 0.86^{+0.30}_{-0.38}$ AU^2 s^{-1}	$c = 0.48^{+0.16}_{-0.15}$ AU^2 s^{-1}
$\gamma = 1.42^{+0.63}_{-0.42}$	

Previously, a study on the rigidity dependence of the diffusion coefficient in the heliosheath has been done by Webber et al. (2018). Authors used protons data in a force field approximation framework (Gleeson and Axford, 1968) and found a constant diffusion coefficient below a certain $P = P_{th}$ threshold, while a linear grow above P_{th}. The change in the behaviour at P_{th} is interpreted as a pile-up of the turbulence cascade, which then leads to rigidity dependent diffusion of particles at higher rigidities. The present analysis finds a similar result but includes data from various ions observed by Voyager 1. We find that, in the rigidity range from 0.5 to 1.8 GV, the spectral index of the rigidity dependence is $\gamma = 1.42^{+0.63}_{-0.42}$.

In the end, the final result is affected by different factors. For example the large uncertainties on data and the correlation effects due to particle propagation between the heliosheath and the inner heliosphere.

The inferred diffusion coefficient and especially its spectral index comes from data extrapolated over a very narrow rigidity range, scanning not even one order of magnitude around 1 GV. The obtained value of $\gamma = 1.42$ seems to be between the lowest and highest values proposed in literature for $P < P_{th}$ ($\gamma \sim 0$) and for $P > P_{th}$ ($\gamma \sim 2$) (Jokipii, 1971; Rao, 1972; Caballero-Lopez et al., 2019). The region we are studying is, indeed, supposed to be the threshold region where the behaviour of κ changes, thus we can not expect to directly compare our value with what is found in literature but rather to include our result for the definition of κ in the critical region around P_{th}. What we found is a dependence on the rigidity P, which is reasonably in agreement with what Lang et al. (2024) also found. In their study, which simulates solar energetic protons and electrons in a 1D approach too, the focus is on the parallel component of the diffusion coefficient, which does not seem to show a rigidity dependence if not for the SOHO/HED proton event on 2012 May 17 (in agreement with Droge (2000)). Their conclusions lead to the need for a more comprehensive modeling of the dissipation range of the turbulence and larger-scale plasma parameters (Engelbrecht et al., 2022), which would enhance the results reliability for the perpendicular component as well. Els et al. (2024), using proton particles, study both of the diffusion tensor components and find the
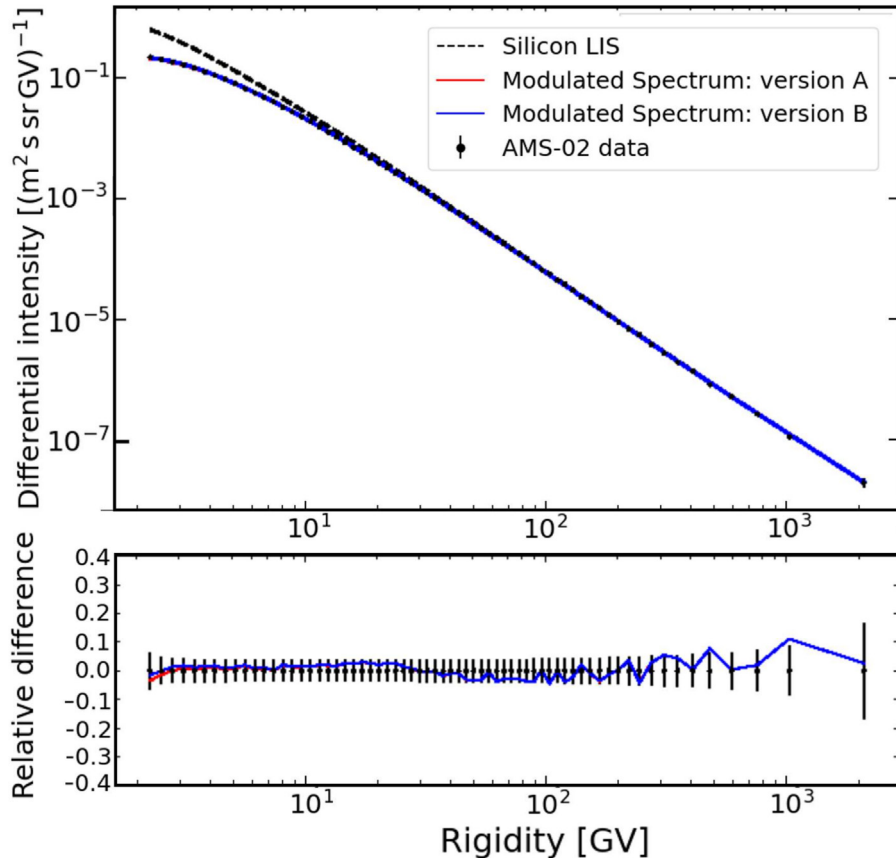

Fig. 5. Modulated spectrum at 1AU for Si ions using in the heliosheath the linear (version A) and powel law (version B) function. The data are those from AMS-02 (Aguilar et al., 2020).

perpendicular one to be rigidity independent too and roughly an order of magnitude below the Palmer consensus (Palmer, 1982), which suggests that the consensus can be considered as an upper limit (in agreement with Zhang et al. (2007) and Engelbrecht et al. (2022)). The simulated values for this component seem to agree with the Field Line Random Walk (FLRW) and the Non Linear Guiding Center (NLGC) theories for the diffusive mean free paths (look at Els et al. (2024) for the detailed expressions). Their mean free paths ratio $\lambda_\perp/\lambda_\parallel$ shows a marked decrease, as also reported by Dundovic et al. (2020). All of these studies have been performed at 1 AU, so while in their case the comparison with the Palmer consensus comes naturally and consistently, in ours it provides some range of reference with respect to an effective diffusion coefficient obtained at way higher distances from Earth. Moreover, for Lang et al. (2024), the considered energy range spans more than 2 orders of magnitude, which is much larger than our case. To improve the accuracy of the parameters derived within the present approach it would be very useful to include data at higher rigidities. A much stronger experimental effort in amplifying the energetic range of detected CRs in the heliosheath area is then needed. Another point worth mentioning is that most of the nature of the heliosheath is still unknown and debatable. Having more insights on the geometry of such a complicated region would certainly improve the understanding of propagation and diffusion, thus allow us to constrain it in a more precise way.

More experimental constraints related both to plasma and cosmic ray measurements are expected in the future from missions in the outer heliosphere such as the New Horizons mission (Hill et al., 2020; McComas et al., 2021) which is supposed to cross the termination shock in a few years or the proposed Interstellar Probe mission (Brandt et al., 2023; Dialynas et al., 2023).

Declaration of Competing Interest

The authors declare that they have no known competing financial interests or personal relationships that could have appeared to influence the work reported in this paper.

Acknowledgements

Appendix A.

In two dimensions, the used coordinates for the description of diffusion are r and θ. The diffusion tensor describing diffusion in a magnetic field B is:

$$K_{rr} = K_{\perp,2} \sin^2 \zeta + \cos^2 \zeta \left(K_\parallel \cos^2 \psi + K_{\perp,3} \sin^2 \psi \right) \qquad (8)$$

$$K_{\theta\theta} = K_{\perp,2} \cos^2 \zeta + \sin^2 \zeta \left(K_\parallel \cos^2 \psi + K_{\perp,3} \sin^2 \psi \right) \qquad (9)$$

$$K_{r\theta} = \sin \zeta \cos \zeta \left(K_\parallel \cos^2 \psi + K_{\perp,3} \sin^2 \psi - K_{\perp,2} \right) \qquad (10)$$

$$K_{\theta r} = \sin \zeta \cos \zeta \left(K_\parallel \cos^2 \psi + K_{\perp,3} \sin^2 \psi - K_{\perp,2} \right) \qquad (11)$$

where $\tan \psi = -(B_\phi/(B_r^2 + B_\theta^2))$ and $\tan \zeta = B_\theta/B_r$. For rigidities P higher than 1 GV, HelMod uses

$$K_\parallel = \frac{\beta}{3} K_0 \left[\frac{P}{1\text{GV}} + g_{\text{low}} \right] \left(1 + \frac{r}{1\text{AU}} \right) \qquad (12)$$

where β is the particle speed in units of speed of light. The parameterizations for K_0, dependent on solar activity and magnetic polarity, can differ (look at Boschini et al. (2018) for details). The perpendicular terms in the equation above are proportional to the parallel one:

$$\frac{K_{\perp,i}}{K_\parallel} = \rho_i \qquad (13)$$

where i stands for r and θ. We use $\rho_i = 0.065$ and $g_{\text{low}} = 0.5$.

Appendix B.

We list here some of the parameterisations used in literature for the parallel and perpendicular mean free paths. Let's start from Lang et al. (2024), where they use, for a slab turbulence (look at Engelbrecht et al. (2022) for details), the following expression for parallel component of the mean free path:

$$\lambda_\parallel = \frac{3}{8} v \int_{-1}^{+1} \frac{(1-\mu^2)^2}{D_{\mu\mu}(\mu)} \mu$$

Here v is the particle speed, $D_{\mu\mu}$ is the pitch-angle diffusion coefficient (look at Droge (2000) for the details on the $D_{\mu\mu}$ parameterization). The perpendicular mean free path in the FLRW theory in a 2D geometry is given by (Strauss et al., 2017)

$$\lambda_\perp = \frac{\sqrt{\delta B_{2D}^2/2}}{B_0} \times \sqrt{C_0 \lambda_{1,2D}^2 \left(\frac{1}{b-1} + \frac{1}{1+\zeta} + \log\left[\frac{\lambda_{0,2D}}{\lambda_{1,2D}} \right] \right)}$$

which does not display a rigidity dependence. In the NLGC theory, instead, the perpendicular component is described, in terms of $\lambda_\parallel$ by (Shalchi et al. (2004), Burger et al. (2008))

$$\lambda_\perp = \left[a^2 \sqrt{3\pi} \frac{\zeta-1}{\zeta/2} \frac{\Gamma(\zeta/2)}{\Gamma(\zeta/2 - 1/2)} \lambda_{1,2D} \frac{\delta B_{2D}^2}{B_0^2} \right]^{2/3} \lambda_\parallel^{1/3},$$

In both cases ζ stands for the spectral index of the turbulence inertial range (for the other details on the parameters of both expressions look at Els et al. (2024)). In the NLGC case, a rigidity dependence of $\sim P^{1/9}$ is observed at low rigidities and one of $\sim P^{2/3}$ at higher rigidities.

Appendix C.

As we test our results for consistency in comparison with the modulated spectra form AMS-02 at 1 AU in Boschini et al. (2019), Boschini et al. (2020), we also use other particles beyond Si ions (as already shown in Fig. 5). Here, we show some modulated spectra using the linear and power law forms for the diffusion coefficient for Mg and O ions too.
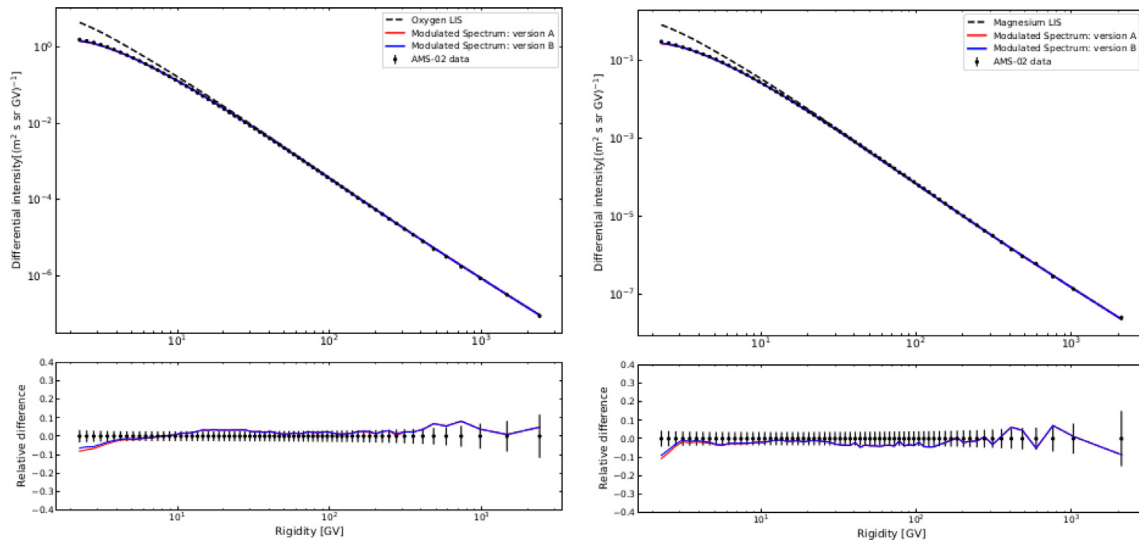
Modulated spectrum at 1 AU for Mg and O ions using in the heliosheath the linear (version A) and power law (version B) function. The data are those from AMS-02 (Aguilar et al. 2020).

References

Aguilar, M., Ali Cavasonza, L., Ambrosi, G., et al., 2020. Properties of neon, magnesium, and silicon primary cosmic rays results from the alpha magnetic spectrometer. Phys. Rev. Lett. 124, 211102. https://doi.org/10.1103/PhysRevLett.124.211102 (AMS Collaboration) URL: https://link.aps.org/doi/10.1103/PhysRevLett.124.211102.

Bobik, P., Boschini, M., Della Torre, S., et al., 2016. On the forward-backward-in-time approach for monte carlo solution of parker's transport equation: one-dimensional case. J. Geophys. Res.-Space 121 (5), 3920–3930. https://doi.org/10.1002/2015JA022237, URL: https://agupubs.onlinelibrary.wiley.com/doi/full/10.1002/2015JA022237.

Borovikov, S.N., Pogorelov, N.V., Burlaga, L.F., et al., 2011. Plasma near the heliosheath: observations and modeling. Astrophys. J. Lett. 728 (1), L21. https://doi.org/10.1088/2041-8205/728/1/L21.

Borovikov, S.N.e.a., 2008. Consequences of the heliopause instability caused by charge exchange. Astrophys. J. 682 (2), 1404. https://doi.org/10.1086/589634, URL: https://iopscience.iop.org/article/10.1086/589634.

Borovikov, S.N.e.a., 2012. Solar rotation effects on the heliosheath flow near solar minima. Astrophys. J. 750 (1), 42. https://doi.org/10.1088/0004-637X/750/1/42, URL: https://iopscience.iop.org/article/10.1088/0004-637X/750/1/42.

Boschini, M., Della Torre, S., Gervasi, M., et al., 2017. Solution of heliospheric propagation: unveiling the local interstellar spectra of cosmic-ray species. ApJ 840 (2), 115. https://doi.org/10.3847/1538-4357/aa6e4f, URL: https://iopscience.iop.org/article/10.3847/1538-4357/aa6e4f.

Boschini, M., Della Torre, S., Gervasi, M., et al., 2020. Inference of the local interstellar spectra of cosmic-ray nuclei z < 28 with the GalProp-HelMod framework. Astrophys. J. Suppl. 250 (2), 27. https://doi.org/10.3847/1538-4365/aba901, URL: https://iopscience.iop.org/article/10.3847/1538-4365/aba901.

Boschini, M., Della Torre, S., Gervasi, M. et al., 2018a. Helmod in the works: from direct observations to the local interstellar spectrum of cosmic-ray electrons. ApJ, https://iopscience.iop.org/article/10.3847/1538-4357/aaa75e.

Boschini, M., Della Torre, S., Gervasi, M., et al., 2020. Deciphering the local interstellar spectra of secondary nuclei with the galprop/helmod framework and a hint for primary lithium in cosmic rays. Astrophys. J. 889 (2), 167. https://doi.org/10.3847/1538-4357/ab64f1, URL: https://iopscience.iop.org/article/10.3847/1538-4357/ab64f1.

Boschini, M., Della Torre, S., Gervasi, M. et al. (2018b). Propagation of cosmic rays in heliosphere: The helmod model. Adv. Space Res., 62 (10), 2859–2879. https://www.sciencedirect.com/science/article/pii/S0273117717302971.

Boschini, M.J., Della Torre, S., Gervasi, M., et al., 2019. The helmod model in the works for inner and outer heliosphere: From ams to voyager probes observations. Adv. Space Res. 64 (12), 2459–2476. https://doi.org/10.1016/j.asr.2019.04.007.

Brandt, P.C., Provornikova, E., Bale, S.D., et al., 2023. Future Exploration of the Outer Heliosphere and Very Local Interstellar Medium by Interstellar Probe. Space Sci. Rev. 219 (2), 18. https://doi.org/10.1007/s11214-022-00943-x, URL: https://link.springer.com/article/10.1007/s11214-022-00943-x.

Burger, R., Krüger, T., Hitge, M., et al., 2008. A fisk-parker hybrid heliospheric magnetic field with a solar-cycle dependence. Astrophys. J. 674 (1), 511. https://doi.org/10.1086/525039, URL: https://iopscience.iop.org/article/10.1086/525039.

Burlaga, L.F., Ness, N.F., Acuña, M.H., 2007. Magnetic fields in the heliosheath and distant heliosphere: voyager 1 and 2 observations

during 2005 and 2006. Astrophys. J. 668 (2), 1246–1258. https://doi.org/10.1086/521349, URL: https://iopscience.iop.org/article/10.1086/521349.

Caballero-Lopez, R., Engelbrecht, N., Richardson, J., 2019. Correlation of long-term cosmic-ray modulation with solar activity parameters. Astrophys. J. 883 (1), 73. https://doi.org/10.3847/1538-4357/ab3c57, URL: https://iopscience.iop.org/article/10.3847/1538-4357/ab3c57.

Cummings, A., Stone, E., Heikkila, B., et al., 2016. Galactic cosmic rays in the local interstellar medium: Voyager 1 observations and model results. Astrophys. J. 831 (1), 18. https://doi.org/10.3847/0004-637X/831/1/18.

Dialynas, K., Brandt, P.C., Burlaga, L., et al., 2023. A future interstellar probe on the dynamic heliosphere and its interaction with the very local interstellar medium. BAAS 55 (3). https://doi.org/10.3847/25c2cfeb.e3624787.

Droge, M., 2000. The rigidity dependence of solar particle scattering mean free paths. Astrophys. J. 537, 1073–1079. https://doi.org/10.1086/309080, URL: https://iopscience.iop.org/article/10.1086/309080.

Dundovic, A., Pezzi, O., Blasi, P., et al., 2020. Novel aspects of cosmic ray diffusion in synthetic magnetic turbulence. Phys. Rev. D 102 (10), 103016. https://doi.org/10.1103/PhysRevD.102.103016, URL: https://link.aps.org/doi/10.1103/PhysRevD.102.103016.

Els, P., Engelbrecht, N., Lang, J., et al., 2024. The diffusion tensor of protons at 1 au: Comparing simulation, observation, and theory. Astrophys. J. 975 (1), 134. https://doi.org/10.3847/1538-4357/ad7c44, URL: https://iopscience.iop.org/article/10.3847/1538-4357/ad7c44.

Engelbrecht, N.E., Di Felice, V., 2020. Uncertainties implicit to the use of the force-field solutions to the Parker transport equation in analyses of observed cosmic ray antiproton intensities. Phys. Rev. D, 102(10), 103007. doi:10.1103/PhysRevD.102.103007.

Engelbrecht, N.E., Effenberger, F., Florinski, V., et al., 2022. Theory of cosmic ray transport in the heliosphere. Space Sci. Rev. 218 (4), 33. https://doi.org/10.1007/s11214-022-00896-1, URL: https://link.springer.com/article/10.1007/s11214-022-00896-1.

Engelbrecht, N.E., Vogt, A., Herbst, K., et al., 2022. Revisiting the revisited palmer consensus: new insights from jovian electron transport. Astrophys. J. 929 (1), 8. https://doi.org/10.3847/1538-4357/ac58f5, URL: https://iopscience.iop.org/article/10.3847/1538-4357/ac58f5/meta.

Fahr, H., Neutsch, W., Grzedzielski, S., et al., 1986. Plasma transport across the heliopause. Space Sci. Rev. 43 (3), 329–381. https://doi.org/10.1007/BF00190639, URL: https://link.springer.com/article/10.1007/BF00190639.

Florinski, V., Zank, G., Pogorelov, N., 2003. Galactic cosmic ray transport in the global heliosphere. J. Geophys. Res.: Space Phys. 108 (A6). https://doi.org/10.1029/2002JA009695, URL: https://agu-pubs.onlinelibrary.wiley.com/doi/full/10.1029/2002JA009695.

Fraternale, F., Adhikari, L., Fichtner, H., et al., 2022. Turbulence in the outer heliosphere. Space Sci. Rev. 218 (6), 50. https://doi.org/10.1007/s11214-022-00914-2, URL: https://link.springer.com/article/10.1007/s11214-022-00914-2.

Gleeson, L., Axford, W., 1968. Solar modulation of galactic cosmic rays. ApJ 154, 1011. https://doi.org/10.1086/149822.

Goldstein, M., Wicks, R., Perri, S., et al., 2015. Kinetic scale turbulence and dissipation in the solar wind: key observational results and future outlook. Phil. Trans. R. Soc. London, Ser. A 373 (2041). https://doi.org/10.1098/rsta.2014.0147, 20140147. URL: https://royalsocietypublishing.org/doi/full/10.1098/rsta.2014.0147.

Goodman, J., Weare, J., 2010. Ensemble samplers with affine invariance. Commun. Appl. Math. Comput. Sci. 5 (1), 65–80. https://doi.org/10.2140/camcos.2010.5.65.

Hill, M.E., Allen, R.C., Kollmann, P., et al., 2020. Influence of solar disturbances on galactic cosmic rays in the solar wind, heliosheath, and local interstellar medium: advanced composition explorer, new horizons, and voyager observations. Astrophys. J. 905 (1), 69. https://doi.org/10.3847/1538-4357/abb408, URL: https://iopscience.iop.org/article/10.3847/1538-4357/abb408.

Hosteaux, S., Rodriguez, L., & Poedts, S. (2022). Analysis of voyager 1 and voyager 2 in situ cme observations. Adv. Space Res., 70(6), 1684–1719. https://www.sciencedirect.com/science/article/pii/S0273117722001910. doi:10.1016/j.asr.2022.03.005.

Huang, S., Sahraoui, F., Andrés, N., et al., 2021. The ion transition range of solar wind turbulence in the inner heliosphere: parker solar probe observations. ApJL 909 (1), L7. https://doi.org/10.3847/2041-8213/abdaaf, URL: https://iopscience.iop.org/article/10.3847/2041-8213/abdaaf.

Jokipii, J.R., 1971. Propagation of cosmic rays in the solar wind. Geophys. Rev. 9 (1), 27–87. https://doi.org/10.1029/RG009i001p00027.

Kleimann, J., Dialynas, K., Fraternale, F., et al., 2022. The structure of the large-scale heliosphere as seen by current models. Space Sci. Rev. 218 (4), 36. https://doi.org/10.1007/s11214-022-00902-6, URL: https://link.springer.com/article/10.1007/s11214-022-00902-6.

Kurth, W., Burlaga, L., Kim, T., et al., 2023. Voyager observations of electron densities in the very local interstellar medium. Astrophys. J. 951 (1), 71. https://doi.org/10.3847/1538-4357/acd44c, URL: https://iopscience.iop.org/article/10.3847/1538-4357/acd44c.

Lang, J., Strauss, R., Engelbrecht, N., et al., 2024. A detailed survey of the parallel mean free path of solar energetic particle protons and electrons. Astrophys. J. 971 (1), 105. https://doi.org/10.3847/1538-4357/ad55c3, URL: https://iopscience.iop.org/article/10.3847/1538-4357/ad55c3.

Langner, U., Potgieter, M., 2005. Modulation of galactic protons in an asymmetrical heliosphere. Astrophys. J. 630 (2), 1114. https://doi.org/10.1086/431547, URL: https://iopscience.iop.org/article/10.1086/431547.

Lemoine, M., 2023. Particle transport through localized interactions with sharp magnetic field bends in MHD turbulence. J. Plasma Phys. 89 (5), 175890501. https://doi.org/10.1017/S0022377823000946.

Lista, L. et al., 2017. Statistical methods for data analysis in particle physics volume 941. Springer. https://doi.org/10.1007/978-3-319-20176-4.

Low, B., 2019. Coronal magnetism as a universal phenomenon. Elsevier. https://doi.org/10.1016/B978-0-12-814334-6.00008-X.

Luo, X., Zhang, M., Potgieter, M., et al., 2015. A numerical simulation of cosmic-ray modulation near the heliopause. Astrophys. J. 808 (1), 82. https://doi.org/10.1088/0004-637X/808/1/82, URL: https://iopscience.iop.org/article/10.1088/0004-637X/808/1/82.

Manuel, R., Ferreira, S.E.S., Potgieter, M.S., 2014. Time-dependent modulation of cosmic rays in the heliosphere. Sol. Phys. 289 (6), 2207–2231. https://doi.org/10.1007/s11207-013-0445-y, URL: https://link.springer.com/article/10.1007/s11207-013-0445-y. arXiv:1310.5514.

McComas, D., Ebert, R., Elliott, H., et al., 2008. Weaker solar wind from the polar coronal holes and the whole sun. Geophys. Res. Lett. 35 (18). https://doi.org/10.1029/2008GL034896.

McComas, D.J., Swaczyna, P., Szalay, J.R., et al., 2021. Interstellar pickup ion observations halfway to the termination shock. Astrophys. J. Suppl. 254 (1), 19. https://doi.org/10.3847/1538-4365/abee76, URL: https://iopscience.iop.org/article/10.3847/1538-4365/abee76.

Moraal, H., 2013. Cosmic-ray modulation equations. Space Sci. Rev. 176 (1), 299–319. https://doi.org/10.1007/s11214-011-9819-3, URL: https://link.springer.com/article/10.1007/s11214-011-9819-3.

Palmer, I., 1982. Transport coefficients of low-energy cosmic rays in interplanetary space. Rev. Geophys. 20 (2), 335–351. https://doi.org/10.1029/RG020i002p00335.

Parker, E., 1965. A brief outline of the development of cosmic ray modulation theory. ICRC 1, 26.

Pine, Z.B., Smith, C.W., Hollick, S.J. et al. (2020a). Solar Wind Turbulence from 1 to 45 au. I. Evidence for Dissipation of Magnetic Fluctuations Using Voyager and ACE Observations. The Astrophysical Journal, 900(2), 91. doi:10.3847/1538-4357/abab10.

Pine, Z.B., Smith, C.W., Hollick, S.J. et al. (2020b). Solar Wind Turbulence from 1 to 45 au. II. Analysis of Inertial-range Fluctuations Using Voyager and ACE Observations. The Astrophysical Journal, 900(2), 92. doi:10.3847/1538-4357/abab0f.

Pine, Z.B., Smith, C.W., Hollick, S.J. et al. (2020c). Solar Wind Turbulence from 1 to 45 au. III. Anisotropy of Magnetic Fluctuations in the Inertial Range Using Voyager and ACE Observations. The Astrophysical Journal, 900(2), 93. doi:10.3847/1538-4357/abab11.

Pine, Z.B., Smith, C.W., Hollick, S.J. et al. (2020d). Solar Wind Turbulence from 1 to 45 au. IV. Turbulent Transport and Heating of the Solar Wind Using Voyager Observations. The Astrophysical Journal, 900(2), 94. doi:10.3847/1538-4357/abab12.

Pine, Z.B., Smith, C.W., Hollick, S.J. et al. (2020e). Solar Wind Turbulence from 1 to 45 au. V. Data Intervals from the Voyager Observations. The Astrophysical Journal Supplement, 250(1), 14. doi:10.3847/1538-4365/abab0e.

Potgieter, M.S., 2013. Solar modulation of cosmic rays. Living Rev. Sol. Phys. 10 (1), 3. https://doi.org/10.12942/lrsp-2013-3. arXiv:1306.4421, URL: https://link.springer.com/article/10.12942/lrsp-2013-3.

Rankin, J., Bindi, V., Bykov, A., et al., 2022. Galactic cosmic rays throughout the heliosphere and in the very local interstellar medium. Space Sci. Rev. 218 (5). https://doi.org/10.1007/s11214-022-00912-4, URL: https://link.springer.com/article/10.1007/s11214-022-00912-4.

Rao, U., 1972. Solar modulation of galactic cosmic radiation. Space Sci. Rev. 12 (6), 719–809. https://doi.org/10.1007/BF00173071.

Reichherzer, P., Becker Tjus, J., Zweibel, E.G., et al., 2020. Turbulence-level dependence of cosmic ray parallel diffusion. Mon. Not. R. Astron. Soc. 498 (4), 5051–5064. https://doi.org/10.1093/mnras/staa2533.

Reichherzer, P., Becker Tjus, J., Zweibel, E.G., et al., 2022. Anisotropic cosmic ray diffusion in isotropic Kolmogorov turbulence. Mon. Not. R. Astron. Soc. 514 (2), 2658–2666. https://doi.org/10.1093/mnras/stac1408.

Reichherzer, P., Bott, A.F., Ewart, R.J. et al. (2025). Efficient micromirror confinement of sub-teraelectronvolt cosmic rays in galaxy clusters. Nature Astronomy, (pp. 1–11). URL: https://www.nature.com/articles/s41550-024-02442-1. doi:10.1038/s41550-024-02442-1.

Richardson, J., Burlaga, L., 2013. The solar wind in the outer heliosphere and heliosheath. Space Sci. Rev. 176, 217–235. https://doi.org/10.1007/s11214-011-9825-5, URL: https://link.springer.com/article/10.1007/s11214-011-9825-5.

Richardson, J.D. (2013). Voyager observations of the interaction of the heliosphere with the interstellar medium. Journal of Advanced Research, 4(3), 229–233. URL: https://www.sciencedirect.com/science/article/pii/S2090123212000896. doi:10.1016/j.jare.2012.09.002. Special Issue on Heliospheric Physics during and after a deep solar minimum.

Salvatore (2023). Inferring the diffusion coefficient in the heliosheath by time spectra simulations of GCRs in the HelMod framework.

Scherer, K., Fichtner, H., Strauss, R.D., et al., 2011. On cosmic ray modulation beyond the heliopause: Where is the modulation boundary?. ApJ 735 (2), 128. https://doi.org/10.1088/0004-637X/735/2/128, URL: https://iopscience.iop.org/article/10.1088/0004-637X/735/2/128.

Shalchi, A., Bieber, J., Matthaeus, W., 2004. Analytic forms of the perpendicular diffusion coefficient in magnetostatic turbulence. Astrophys J 604 (2), 675. https://doi.org/10.1086/382128, URL: https://iopscience.iop.org/article/10.1086/382128.

Sokół, J.M., Kucharek, H., Baliukin, I.I. et al. ( ). Interstellar neutrals, pickup ions, and energetic neutral atoms throughout the heliosphere: present theory and modeling overview. Space Science Reviews,. doi:10.1007/s11214-022-00883-6.

Song, X., Luo, X., Potgieter, M.S. et al. (2022). Comprehensive modulation potential for the solar modulation of galactic cosmic rays. Phys. Rev. D, 106, 123004. URL: https://journals.aps.org/prd/abstract/10.1103/PhysRevD.106.123004. doi:10.1103/PhysRevD.106.123004.

Stone, E.C., Cummings, A.C., McDonald, F.B., et al., 2013. Voyager 1 observes low-energy galactic cosmic rays in a region depleted of heliospheric ions. Science 341 (6142), 150–153. https://doi.org/10.1126/science.1236408.

Strauss, R., Effenberger, F., 2017. A hitch-hiker's guide to stochastic differential equations. Space Sci. Rev. 212 (1), 151–192. https://doi.org/10.1007/s11214-017-0351-y, URL: https://link.springer.com/article/10.1007/s11214-017-0351-y.

Strauss, R.D.T., Dresing, N., Engelbrecht, N.E., 2017. Perpendicular diffusion of solar energetic particles: model results and implications for electrons. Astrophys. J. 837 (1), 43.

Strong, A.W., Moskalenko, I.V., 1998. Propagation of Cosmic-Ray Nucleons in the Galaxy. Astrophys J 509 (1), 212–228. https://doi.org/10.1086/306470, URL: https://iopscience.iop.org/article/10.1086/306470.

Tjus, J.B., & Merten, L. (2020). Closing in on the origin of galactic cosmic rays using multimessenger information. Physics Reports, 872, 1–98. URL: https://www.sciencedirect.com/science/article/pii/S0370157320301927. doi:10.1016/j.physrep.2020.05.002.

Webber, W.R., Harrison, T.E., Lal, N. et al. (2018). The rigidity dependence of the diffusion coefficient in the heliosheath and an explanation of the extreme solar modulation effects for cosmic ray electrons from 3–60 mev observed at voyager 1. arXiv preprint arXiv:1810.07154. URL: https://arxiv.org/abs/1810.07154. doi:10.48550/arXiv.1810.07154.

Zank, G., 1999. Interaction of the solar wind with the local interstellar medium: A theoretical perspective. Space Sci. Rev. 89 (3), 413–688. https://doi.org/10.1023/A:1005155601277, URL: https://link.springer.com/article/10.1023/A:1005155601277.

Zhang, M., Luo, X., Pogorelov, N., 2015. Where is the cosmic-ray modulation boundary of the heliosphere?. Phys. Plasmas 22 (9), 091501. https://doi.org/10.1063/1.4928945.

Zhang, M., Qin, G., Rassoul, H. et al. (2007). Ulysses observations of jovian relativistic electrons in the interplanetary space near jupiter: Determination of perpendicular particle transport coefficients and their energy dependence. Planetary and Space Science, 55(1–2), 12–20. URL: https://www.sciencedirect.com/science/article/abs/pii/S0032063305002308. doi:/10.1016/j.pss.2005.11.004.

Zirnstein, E.J., Möbius, E., Zhang, M., et al., 2022. In situ observations of interstellar pickup ions from 1 au to the outer heliosphere. Space Sci. Rev. 218 (4), 28. https://doi.org/10.1007/s11214-022-00895-2, URL: https://link.springer.com/article/10.1007/s11214-022-00895-2.